Distribution of energy deposited by a moderately intense 26-MeV electron beam in thick metal targets

A. Stolovy, J. M. Kidd, A. I. Namenson, M. I. Haftel, G. H. Herling, and J. B. Aviles, Jr.
Naval Research Laboratory, Washington, D.C. 20375-5000
(Received 23 March 1989)

Experiments have been performed with the moderately intense electron-beam pulses (8 kA/cm^2 peak) at the Los Alamos National Laboratory pulsed high-energy radiographic machine emitting x-rays (PHERMEX) facility and with the much weaker beam at the Naval Research Laboratory linac, to measure energy absorption in Al, Ti, and W targets. The energy spectra at the two facilities were similar, with an average energy of about 26 MeV. A calorimetric method was used to measure the deposited energy. The experimental results are compared to each other and to Monte Carlo integrated "tiger" system (ITS) code calculations. Calorimeters consisting of two and four sections were used. The linac data were in good agreement with single-electron code calculations. Evidence for collective effects appears as a redistribution of the absorbed energy in the PHERMEX data, although the beam intensity is very much lower than in previous investigations of this effect.

I. INTRODUCTION

In recent years, there has been a lot of interest in the phenomenon of anomalously large energy deposition by an intense beam of charged particles incident on a solid target. The interest has been spurred by the application to thermonuclear fusion problems. Several experiments have been performed with intense electron-beam pulses to demonstrate the effect.[1-3] In these experiments, the electron energy was 0.5–1 MeV, the targets were very thin (10–100 μm), and beam current densities on target were very high (10^6–10^7 A/cm^2). Under these conditions, enhancements of 5–10 over single-electron stopping power calculations were observed. Enhanced stopping power has also been observed with intense deuteron[4] and molecular-ion[5,6] beams.

Theoretical work has provided several collective mechanisms by which a very intense electron beam could produce such an effect: self-induced magnetic and electric fields which result in beam stagnation,[7-10] the beam-density effect and related wake effects,[11-13] temperature and plasma-density (or ionization) effects,[14] and two-stream plasma instability effects.[3,15] Some of these effects are interrelated; the references cited are only an appropriate sampling of the large amount of theoretical work which has been done.

The main purposes of this work are to see if enhanced energy deposition due to collective effects is observable at electron-beam intensities which are two to three orders of magnitude lower than in any previous such investigation, and to obtain the distribution of deposited energy in thick targets, using a much higher energy beam (26 MeV) than used previously. We have made quantitative measurements of energy deposition in Al, Ti, and W targets with weak (5 A/cm^2) and relatively intense (8 kA/cm^2) electron beams at two facilities. At these intensities, the plasma-related effects given above are probably not applicable.

Since the energy absorbed by the target is rapidly distributed, we have used a calorimetric technique to measure the deposited energy in sectioned targets. The energy deposited is obtained from the product of the mass, specific heat, and observed temperature rise. Measurements were made with relatively high-intensity beam pulses at the Los Alamos National Laboratory (LANL) pulsed high-energy radiographic machine emitting x-rays (PHERMEX), and with low-intensity beam pulses at the Naval Research Laboratory (NRL) linac. Monte-Carlo electron-photon shower code [integrated tiger system or ITS (Ref. 16)] calculations were also made, and were compared to both sets of experimental results. The same average beam energy was used at the two facilities.

II. EXPERIMENTAL DESCRIPTION

A. Two-section calorimeters

The first series of experiments was done on calorimeter assemblies consisting of two insulated sections: a sample section thick enough to absorb one-fourth to one-half of the incident electron energy, and a copper beam stop section more than thick enough to absorb the rest of the electron energy. An illustration of this cylindrical assembly is shown in Fig. 1. The sections are tapered to catch

TABLE I. Characteristics of two-section calorimeter assemblies. Specific heats for Al, Ti, and Cu are 0.216, 0.125, and 0.0925 cal/g °C, respectively. All Cu beam stops were 1.91 cm thick.

Calorimeter	Material	Thickness (cm)	Mass (g)	Cu beam stop mass (g)
1	Al	0.635	7.69	174.41
2	Al	1.27	17.60	207.35
3	Ti	0.635	13.08	174.58
4	Ti	1.27	29.35	206.25

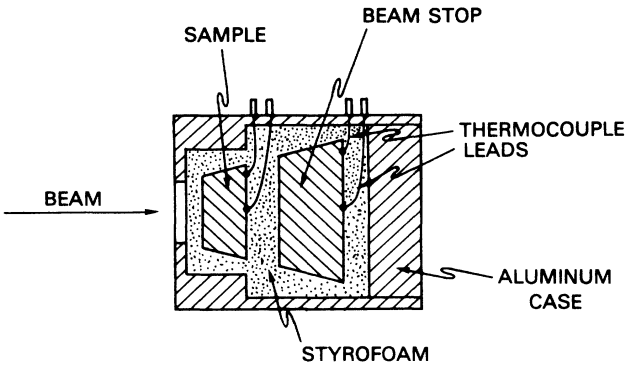

FIG. 1. Two-section calorimeter assembly consisting of a tapered sample and a tapered copper beam stop, with attached thermocouples (cylindrical geometry).

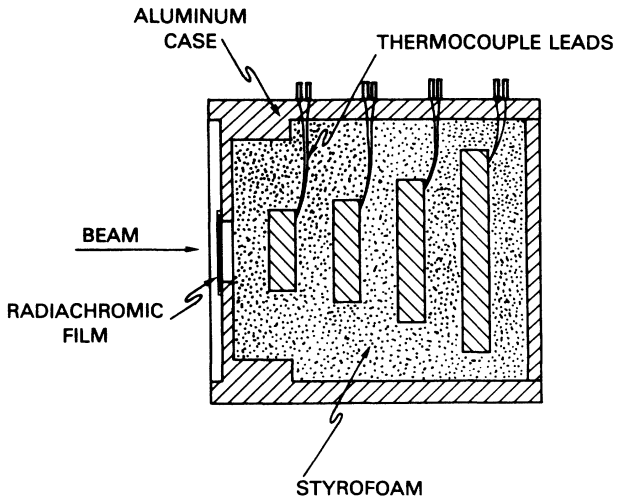

FIG. 2. Four-section calorimeter assembly consisting of four disks of the same metal, with attached thermocouples (cylindrical geometry).

the scattered electrons while minimizing mass. Some of the bremsstrahlung produced is absorbed farther downstream, but much of it escapes the system. As shown, two Chromel-Alumel (0.0127-cm-diam) thermocouples are screwed to both the sample and Cu beam stop, one at the center and one at the edge. This allows us to observe the spatial distribution of the deposited energy as a function of time until thermal equilibrium is established. Four modules of this type were made, including two thicknesses of type 6061 aluminum alloy and two thicknesses of titanium alloy (6 wt. %. Al, 4 wt. % V). The thicknesses, masses, and specific heats of the materials used in these four calorimeters are listed in Table I.

The sections are imbedded in styrofoam to isolate them thermally. In this way, we have separated a region where the beam current density is intense (in the Al or Ti sample), from a region where it is much weaker (in the Cu beam stop) due to beam spreading. The energy absorbed in each section is the product of the mass, specific heat (given in Table I), and the observed temperature rise. The latter is obtained from the average of the equilibrium temperatures for the two thermocouples attached to each section.

The same calorimeters were exposed at the linac and PHERMEX facilities. The ratio of the energy absorbed in the Al or Ti sample to the energy absorbed in the beam stop should then be a parameter that would be sensitive to any difference in absorption in the two sections at the two facilities.

B. Four-section calorimeters

In order to study the energy deposition in metals in more detail, we constructed three calorimeter assemblies, each of which had four sections, as shown in Fig. 2. The first assembly contained aluminum sections; the second, titanium sections; and the third, tungsten sections, in order to look for a possible Z dependence. In each case, the total thickness is about 20% greater than the continuous slowing down approximation range[17] of the maximum beam electron energy, to ensure that all the electrons are

TABLE II. Characteristics of four-section calorimeters.

Material	Specific heat (cal g^{-1} °C^{-1})	Section	Thickness (cm)	Mass (g)
Al	0.216	1	1.52	21.46
		2	1.27	27.28
		3	1.27	53.23
		4	1.27	108.40
Ti	0.125	1	0.79	17.42
		2	0.79	28.32
		3	0.79	55.36
		4	0.79	113.37
W	0.033	1	0.16	14.97
		2	0.16	23.10
		3	0.16	44.84
		4	0.16	91.46

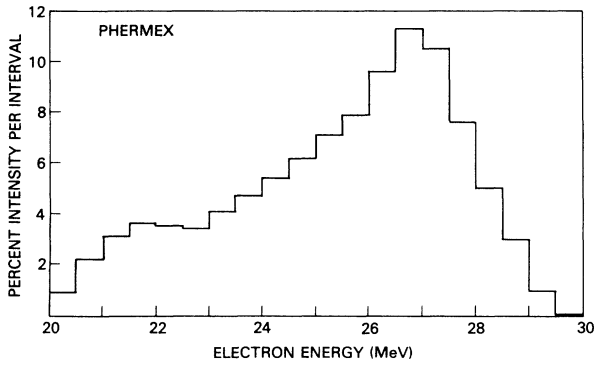

FIG. 3. Energy spectrum of the PHERMEX beam.

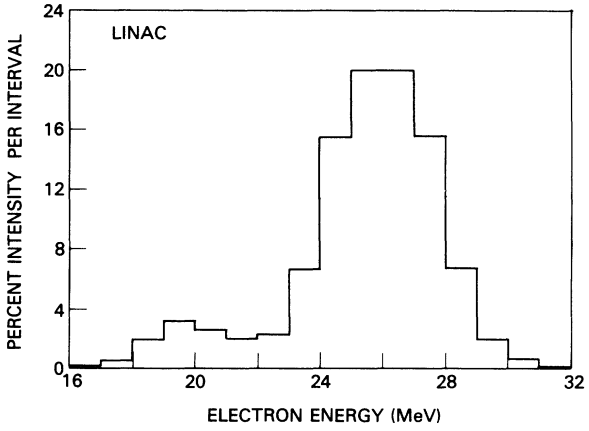

FIG. 4. Energy spectrum of the linac beam.

stopped. The sections again are imbedded in styrofoam to provide thermal isolation, and each has a Chromel-Alumel thermocouple (0.0127 cm diam) attached near the edge. All of the calorimeters were exposed to beam pulses at the two accelerator facilities. Thus we were able to compare energy depth profiles for high-intensity and low-intensity beams with each other, and with Monte Carlo code calculations. The masses, thicknesses, and specific heats of the four-section calorimeters are given in Table II.

C. Accelerator characteristics

The NRL linac produces electron-beam macropulses with the following average characteristics: 10–60 MeV, 0.3 A, 1.5 μs width, and 360 pulses/s. Each of these macropulses consists of many micropulses with the characteristics given in Table III. The PHERMEX produces a single burst of 10 micropulses, with parameters as listed in Table III. Because of both more peak current and a smaller beam area, it is seen that the peak micropulse current density at PHERMEX is about 1500 times that at the linac. It is this large difference in intensity that enabled us to search for a difference in absorption in solid targets. We used metal targets because they come to thermal equilibrium in a few seconds, allowing the use of a simple calorimetric method of measurement.

Both accelerators produce electron beams with a spread of energies. The energy spectrum of the PHERMEX beam, with an average energy of 26 MeV, has been measured with a magnetic spectrometer;[18] it is shown in Fig. 3. Similarly, we have measured the linac beam spectrum at an average energy of 26 MeV with a magnetic spectrometer and radiachromic film as a detector; the results are shown in Fig. 4. Fortunately, the shapes of these spectra are quite similar; each exhibits a peak with a long low-energy tail. The ratio of full width at half peak maximum to average energy is about 15% in both cases. The Monte Carlo code calculations were done using the appropriate spectra for input. A few calculations were done with the spectra delibrately switched, which produced only small changes in the results (1–4 %). This is certainly fortunate, because the depth-deposition profile is dependent upon the incident spectrum. The similarity of the spectra allows us to compare the results obtained at the two facilities directly.

D. Procedure

Signals from the Chromel-Alumel thermocouples are routed through high-gain amplifiers to a four-channel chart recorder. Equilibrium temperatures are obtained from these temperature versus time records. The observed temperature rise ΔT ranges from about 38 °C (first section of W calorimeter at the PHERMEX) to about 0.05 °C (last section of Al calorimeter at the linac). The uncertainty in these measurements is about 1% for $\Delta T > 1$ °C, and about 10% for $\Delta T < 0.1$ °C.

Although the energy deposited per macropulse at the linac is very low, we obtained satisfactory signal strength by exposing the calorimeters to many macropulses (10–40), and increasing the amplifier gains. Experiments were performed with each of the two- and four-section calorimeters, in two periods, and at both accelerators. During each period, experiments with each module were

TABLE III. Micropulse parameters at the linac and PHERMEX.

Facility	Pulse height (A)	Pulse width (ns)	Pulse spacing (ns)	Beam area[a] (cm^2)	Peak current density (A/cm^2)
Linac	4.2	0.025	0.35	0.80	5.25
PHERMEX	400	3.8	20	0.05	8000

[a]At half maximum.

repeated about six times, and the results averaged.

The calorimeters were irradiated in air, close to the thin exit window at each accelerator (0.254 mm Be at the PHERMEX, 0.025 mm stainless steel at the linac). It is important that the beam interact with as little material as possible before entering the calorimeter; the downstream sections of the calorimeters were very sensitive detectors of bremsstrahlung produced by the beam striking material upstream. Indeed, early data taken with a graphite and steel collimator in the beam were discarded because of the large γ-ray background. Background measurements were made by placing the calorimeters to the side of the beam. With nothing in the beam (except the thin exit window), the background was found to be very small in all cases.

Nylon radiachromic films (which turn blue in proportion to their exposure to the beam) were used to align the calorimeters with the beam center. These films were scanned with an optical densitometer to obtain the beam profiles. The full width at half maximum was found to be 11 mm at the linac, and 2.5 mm at the PHERMEX. These are both much smaller than the diameters of the metal sections.

III. RESULTS

A. Two-section calorimeters

The observed temperature rise and calculated absorbed energy E (using the information in Table I) for the two-section calorimeters are tabulated in Table IV for data obtained at the PHERMEX during two separate observation periods. These tabulated numbers are averages over about six runs each. The uncertainties quoted are standard deviations of the mean; they do not include any sources of systematic error.

It can be seen that the beam intensity was a little lower during the second observation period. This is of no consequence since we are concerned only with the distribution of the deposited energy.

These calorimeters were then exposed to multiple beam pulses at the linac with the average electron-beam energy also set to 26 MeV. No attempt was made to match the total-energy absorption at the PHERMEX, since it is only the distribution we are interested in. The experiments at the linac were also done in two periods; i.e., the reproducibility of the experiments was checked by returning to each accelerator after a time lapse, with the machines reset to their original beam parameters. The results are tabulated in Table V. The uncertainties are standard deviations of the mean.

We now combine the data from the two observation periods, and obtain the ratio between the energy absorbed in each sample to the energy absorbed in the corresponding Cu beam stop. Experimental and calculated (Monte Carlo ITS code) results are given in Table VI. The calculations are based on the calorimeter and beam geometries, and the beam-energy spectra (Figs. 3 and 4). The uncertainties in the calculated ratios given in Table VI are assumed to be about 5%.[19] For the experimental data, the uncertainties reflect observed differences between the two observation periods, as well as standard deviations of the mean.

The linac data are seen to yield ratios which are a little higher than the code calculation predicts, but they differ by less than 25%, indicating that single-electron interactions are a reasonable description for this beam. In contrast, the PHERMEX data yield ratios which are considerably higher than those for the code calculations or the linac results, indicating anomalously large absorption in the Al or Ti sample with this intense beam. The effect is larger in Ti than in Al samples of the same thickness. The largest effect appears in the thicker Ti sample, where the PHERMEX ratio is 63% greater than the linac ratio, and is twice the calculated ratio.

B. Four-section calorimeters

Experiments with four-section calorimeters were also carried out during two observation periods at both facilities, and compared to calculations. The observed average temperature rise and calculated energy deposition in each section of the Al, Ti, and W calorimeters (using the information given in Table II) are listed for the PHERMEX data in Table VII, and for the linac data in Table VIII. The uncertainties given in these tables are standard deviations of the mean. Errors associated with mass measurements or heat capacities are assumed to be very small. Note that the instrumentation is capable of measuring a ΔT as small as 0.1 °C with good accuracy. In

TABLE IV. Observed temperature rise ΔT, and calculated absorbed energy E, for one PHERMEX macropulse into the two-section calorimeters, for two observation periods. Data are averages over several runs. The calorimeter numbers on the column headings refer to the calorimeter numbers in Table I.

Calorimeter	1 Al	1 Cu	2 Al	2 Cu	3 Ti	3 Cu	4 Ti	4 Cu
Period 1								
ΔT (°C)	8.74±0.13	3.78±0.02	7.50±0.19	2.68±0.02	13.62±0.30	3.08±0.02	11.75±0.18	1.31±0.01
E (cal)	14.51±0.22	61.05±0.32	28.53±0.72	51.32±0.39	22.27±0.49	49.80±0.32	43.09±0.67	25.06±0.14
Period 2								
ΔT (°C)	6.78±0.03	3.31±0.05	6.05±0.02	2.01±0.02	12.00±0.13	2.26±0.04	10.04±0.05	0.85±0.01
E (cal)	11.25±0.05	53.47±0.79	23.02±0.09	38.54±0.44	19.62±0.21	36.50±0.65	36.83±0.20	16.25±0.25

TABLE V. Observed temperature rise ΔT, and calculated absorbed energy E, for multiple pulses at the NRL linac into the two-section calorimeters, for the two observation periods. Data are averages over six runs. The calorimeter numbers on the column headings refer to the calorimeter numbers in Table I.

Calorimeter	1 Al	1 Cu	2 Al	2 Cu	3 Ti	3 Cu	4 Ti	4 Cu
Period 1								
ΔT (°C)	1.64±0.05	0.93±0.03	2.00±0.05	0.86±0.03	2.90±0.02	0.88±0.01	2.48±0.11	0.37±0.02
E (cal)	2.73±0.07	15.00±0.51	7.60±0.19	16.47±0.50	4.75±0.04	14.25±0.06	9.08±0.41	7.14±0.41
Period 2								
ΔT (°C)	2.96±0.05	1.78±0.03	2.69±0.01	1.19±0.01	4.87±0.04	1.46±0.01	4.26±0.03	0.71±0.01
E (cal)	4.91±0.08	28.75±0.45	10.21±0.04	22.79±0.08	7.96±0.06	23.64±0.10	15.61±0.10	13.45±0.11

TABLE VI. Measured and calculated ratios of energy absorbed in the sample to that in the Cu beam stop, for the two-section calorimeters.

Calorimeter	Material	Thickness (cm)	ITS code	Linac data	PHERMEX data
1	Al	0.635	0.15±0.01	0.18±0.01	0.23±0.03
2	Al	1.27	0.37±0.02	0.46±0.02	0.58±0.03
3	Ti	0.635	0.29±0.01	0.34±0.01	0.50±0.06
4	Ti	1.27	1.01±0.05	1.23±0.12	2.00±0.30

TABLE VII. Observed temperature rise ΔT and calculated deposited energy E for one PHERMEX macropulse into the four-section calorimeters, for two observation periods. Data are averages over several runs. Uncertainties are standard deviations of the mean.

Calorimeter material	Section	Period 1 ΔT (°C)	Period 1 E (cal)	Period 2 ΔT (°C)	Period 2 E (cal)
Al	1	6.17±0.09	28.62±0.42	6.09±0.11	28.23±0.53
	2	3.41±0.05	20.10±0.30	3.31±0.07	19.50±0.40
	3	0.93±0.02	10.69±0.23	0.79±0.01	9.11±0.11
	4	0.13±0.01	2.93±0.16	0.05±0.01	1.17±0.16
Ti	1	9.71±0.07	21.15±0.16	10.81±0.11	23.53±0.24
	2	5.84±0.04	20.66±0.16	6.18±0.08	21.88±0.29
	3	1.50±0.02	10.36±0.16	1.38±0.02	9.55±0.12
	4	0.20±0.01	2.76±0.18	0.10±0.01	1.39±0.20
W	1	37.68±0.19	18.33±0.09	25.36±0.52	12.34±0.25
	2	22.00±0.18	16.51±0.13	10.70±0.18	8.03±0.14
	3	4.51±0.06	6.58±0.09	1.74±0.03	2.54±0.04
	4	0.87±0.02	2.59±0.05	0.49±0.01	1.45±0.03

TABLE VIII. Observed temperature rise ΔT and calculated deposited energy E for multiple linac pulses into the four-section calorimeters, for two observation periods. Data are averages over several runs. Uncertainties are standard deviations of the mean.

Calorimeter Material	Section	Period 1 ΔT (°C)	Period 1 E (cal)	Period 2 ΔT (°C)	Period 2 E (cal)
Al	1	1.39±0.16	6.44±0.74	5.31±0.03	24.61±0.12
	2	0.78±0.11	4.60±0.65	3.04±0.02	17.91±0.11
	3	0.23±0.05	2.64±0.57	1.00±0.02	11.50±0.17
	4	0.06±0.01	1.40±0.30	0.23±0.01	5.39±0.16
Ti	1	2.47±0.05	5.38±0.11	9.01±0.06	19.62±0.13
	2	1.58±0.03	5.59±0.11	5.47±0.05	19.36±0.18
	3	0.51±0.02	3.53±0.11	1.71±0.02	11.83±0.16
	4	0.10±0.01	1.42±0.17	0.32±0.01	4.53±0.14
W	1	6.10±0.17	2.97±0.08	7.89±0.05	3.84±0.03
	2	4.45±0.13	3.34±0.10	5.18±0.02	3.89±0.01
	3	1.40±0.04	2.04±0.05	1.38±0.02	2.01±0.02
	4	0.33±0.01	0.98±0.03	0.28±0.01	0.83±0.01

TABLE IX. Distribution of energy deposited in the four-section calorimeters for the linac and PHERMEX beams with the average energy set at 26 MeV, and Monte Carlo code calculations for comparison. The numbers listed are fractions of total deposited energy. The uncertainties are standard deviations of the mean.

Calorimeter material	Section	PHERMEX data Period 1	PHERMEX data Period 2	Linac data Period 1	Linac data Period 2	ITS code calculation
Al	1	0.459±0.007	0.487±0.009	0.426±0.049	0.414±0.002	0.391±0.020
	2	0.322±0.004	0.336±0.007	0.308±0.043	0.301±0.002	0.307±0.015
	3	0.171±0.004	0.157±0.002	0.174±0.038	0.194±0.003	0.208±0.010
	4	0.047±0.013	0.020±0.003	0.092±0.007	0.091±0.003	0.094±0.005
Ti	1	0.385±0.003	0.418±0.004	0.338±0.007	0.355±0.002	0.334±0.017
	2	0.376±0.003	0.388±0.005	0.351±0.008	0.350±0.003	0.350±0.018
	3	0.189±0.003	0.169±0.002	0.222±0.007	0.214±0.003	0.231±0.012
	4	0.050±0.003	0.025±0.004	0.089±0.005	0.081±0.003	0.085±0.004
W	1	0.416±0.002	0.506±0.010	0.318±0.009	0.363±0.003	0.352±0.018
	2	0.375±0.003	0.330±0.006	0.357±0.011	0.367±0.001	0.378±0.019
	3	0.150±0.002	0.104±0.001	0.219±0.005	0.190±0.002	0.195±0.010
	4	0.059±0.001	0.060±0.001	0.106±0.003	0.080±0.001	0.076±0.004

TABLE X. Effective collisional stopping powers of three metals for 26 MeV electron pulses at the PHERMEX facility, compared to single-electron values. The units are MeV cm^2/g.

Metal	Two-section calorimeter (0.635 cm thick)	Two-section calorimeter (1.27 cm thick)	Four-section calorimeter (first section)	Single-electron calculation
Al	2.15±0.22	2.20±0.22	2.02±0.20	1.73±0.09
Ti	2.01±0.20	2.02±0.20	1.73±0.17	1.61±0.08
W			1.73±0.17	1.30±0.07

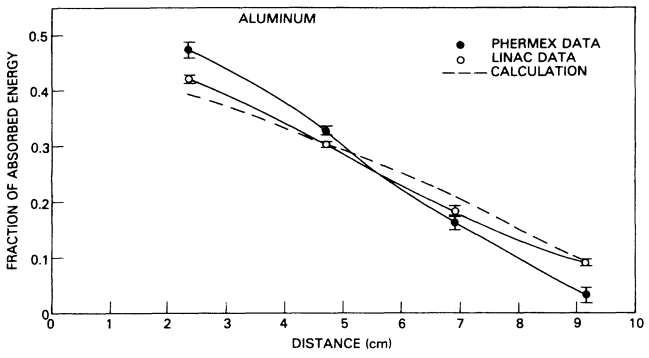

FIG. 5. Comparison of normalized distributions of deposited energy in the four-section Al calorimeter, as measured at the linac and PHERMEX facilities, and as calculated with the ITS code. Distances are from the front face of the calorimeter assembly to the center of each section (Fig. 2). Uncertainty in the calculated curve (dashed line) is about 5%.

some cases, considerable differences can be seen between the data taken in the two PHERMEX observation periods. This is due entirely to differences in accelerator conditions, and gives us a measure of the nonrandom uncertainties associated with these data. The large differences between the data from the two linac observation periods are due primarily to the number of pulses incident on the calorimeters, which varied from 10–40 linac macropulses. Since it is only the distribution of deposited energy we are concerned with, we convert the data in Tables VII and VIII into fractions of total absorbed energy, so that the sum of the fractional energies deposited in the four sections is unity. Values of these normalized data for the two observation periods are given

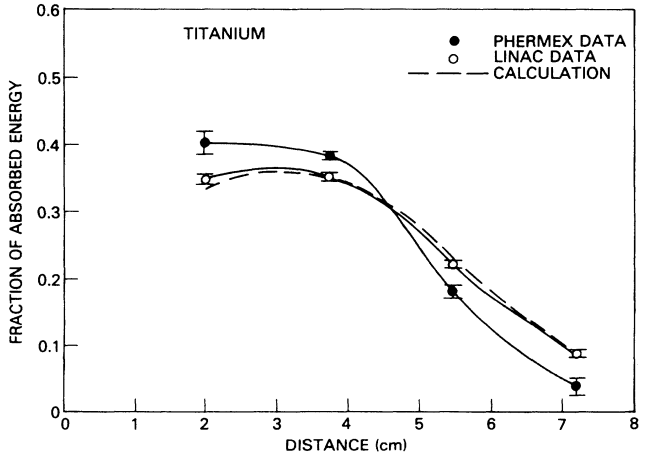

FIG. 6. Comparison of normalized distributions of deposited energy in the four-section Ti calorimeter as measured at the linac and PHERMEX facilities, and as calculated with the ITS code. Distances are from the front face of the calorimeter assembly to the center of each section (Fig. 2). Uncertainty in the calculated curve (dashed line) is about 5%.

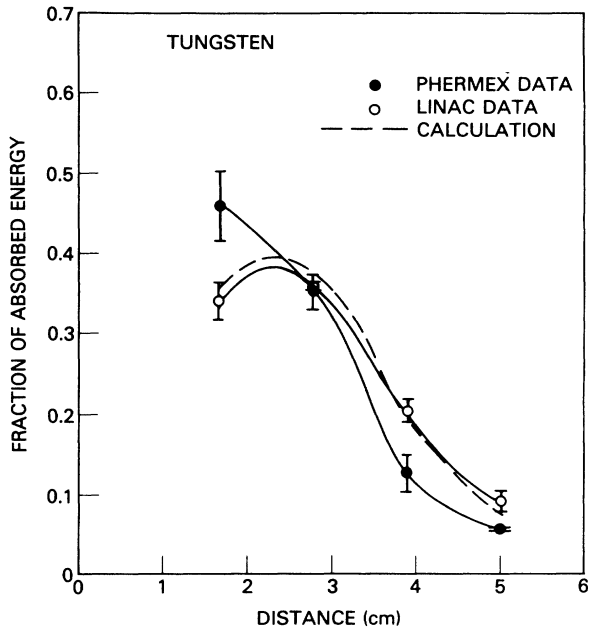

FIG. 7. Comparison of normalized distributions of deposited energy in the four-section W calorimeter as measured at the linac and PHERMEX facilities, and as calculated with the ITS code. Distances are from the front face of the calorimeter assembly to the center of each section (Fig. 2). Uncertainty in the calculated curve (dashed line) is about 5%.

in Table IX, together with ITS code calculated results. The ITS code calculations are assumed to have a 5% uncertainty.[19] The results are also presented in graphical form in Figs. 5, 6, and 7 for tha Al, Ti, and W four-section calorimeters, respectively. The distances plotted are from the front face of the calorimeter to the center of each section (including the 0.95-cm styrofoam thickness between sections).

C. Collisional stopping powers

For some of the PHERMEX data, plots of the micropulse train were obtained for each macropulse, from a calibrated transformer coil. In these cases, we were able to obtain good information on the total input beam current and micropulse width. Combining these data with the measured deposited energy in the section upon which the beam is incident, we can calculated an effective (i.e., average) collisional stopping power S_c. The energy deposited by the beam in this first section is

$$E = \left[\sum I_p\right] \tau \rho t S_c \ , \tag{1}$$

where $\sum I_p$ is the sum of the peak currents of the micropulses, τ is the micropulse width at half maximum, ρ is the sample density, and t is the section thickness. Collisional (nonradiative) effective stopping powers can then be calculated from Eq. (1), using the measured deposited energies in the first section given in Tables IV and VII. The results are listed in Table X, along with single-

electron calculated values at 26 MeV from the tables of Berger and Seltzer,[17] for comparison.

IV. DISCUSSION OF RESULTS

It is clear from an examination of the results in Tables VI and IX, and Figs. 5, 6, and 7, that the PHERMEX data consistently show anomalously strong absorption in the first section (upon which the beam is incident), and reduced absorption in the section farthest downstream. In contrast, the linac data are in good agreement with the single-electron Monte Carlo calculations of the distribution of deposited energy in all of the four-section calorimeters. This represents experimental confirmation of the Monte Carlo code, and also strong evidence that the data taken at the PHERMEX are quite different. Similarly, the effective stopping powers obtained from the PHERMEX data given in Table X are all somewhat larger than the single-electron values. The biggest difference is in the tungsten data, suggesting a possible Z dependence.

To verify these observed effects, it is necessary to apply a statistical test to the results listed in Table IX. If the data follow a known distribution law, then a chi-square test would be appropriate. However, the major source of uncertainty in these experiments is the reproducibility of accelerator conditions in the two periods data were taken at both facilities. Since this type of uncertainty cannot be quantified, it is better to use a distribution-free test.

A simple illustrative test is to normalize the experimental results listed in Table IX for sections 1 and 4 to their code calculated values, and then to rank these normalized values as shown in Table XI. We do not use the data from sections 2 and 3 for this test, since they are in the crossover region (see Figs. 5–7) and are not expected to yield a significant effect. Each of the 12 normalized values at each facility has three attributes: metal type, observation period, and section number. It is seen that the linac data show no dependence on any of its attributes (as would be expected when the data and calculation are in agreement) and the spread in normalized values is rather narrow. For the PHERMEX data, there is no dependence on the metal or observation period, but a clear grouping of the ranked data with respect to section number appears, with a wide distribution of normalized values and a gap between the two groups. The ranking clearly reflects the consistency of the data; i.e., all of the section-4 data absorbed less energy than calculated, while all the section-1 data absorbed more energy than calculated. The probability that this particular ranking of 12 values would occur by chance can be calculated as follows: $(6!)^2/12!=0.11\%$. Therefore, we can say with about 99.9% confidence that the energy distribution observed in the PHERMEX data does not agree with the single-electron calculation, and that the direction of the observed effect is consistent with theories that predict enhanced initial absorption. This confidence would be even greater if we account for the size of the gap between the two ranked groups, and still greater if we also account for the consistent two-section calorimeter data.

Another simple distribution test we could apply is the Wald-Wolfowitz test,[20] which counts the number of runs in the ranked data (a run is a string of data points with the same attribute). Examining the "section" attribute in Table XI, we see that the linac data have six runs and the PHERMEX data have only two runs. If the data were to agree with the single-electron calculation, the number of runs should approximate a normal distribution with a mean of 7 and a standard deviation of 1.73. Therefore, the linac data are in agreement with the calculation, and the PHERMEX data are not.

The only remaining question is: Could the observed effect be due to a mis-setting of the PHERMEX beam parameters to a much lower average energy? Calculations indicate that the PHERMEX data would be reconciled with the code calculations if the average energy had been mis-set to about 23 MeV instead of 26 MeV. However, such a large mis-setting (at two different observation periods) is extremely unlikely.[21] The PHERMEX energy

TABLE XI. Data from Table IX for sections 1 and 4 normalized to their corresponding calculated values, and then ranked.

Linac data				PHERMEX data			
Normalized value	Metal	Observation period	Section	Normalized value	Metal	Observation period	Section
0.903	W	1	1	0.213	Al	2	4
0.965	Ti	2	4	0.294	Ti	2	4
0.968	Al	2	4	0.500	Al	1	4
0.989	Al	1	4	0.588	Ti	1	4
1.012	Ti	1	1	0.776	W	2	4
1.031	W	2	1	0.790	W	1	4
1.040	W	2	4	1.153	Ti	1	1
1.047	Ti	1	4	1.174	Al	1	1
1.059	Al	2	1	1.182	W	1	1
1.063	Ti	2	1	1.246	Al	2	1
1.092	Al	1	1	1.252	Ti	2	1
1.382	W	1	4	1.438	W	2	1

spectrum (Fig. 3) has been carefully measured with a magnetic spectrometer,[18] with an uncertainty of approximately 3%. Code calculations performed within this 3% bound are not compatible with the experimental data. Thus, the only reasonable explanation of the observed data is a collective effect of some kind.

V. CONCLUSION

We have found evidence for anomalous absorption by thick metal targets, using a 26-MeV electron beam with an intensity of about 8 kA/cm^2. An enhancement of 20–30 % in the energy absorbed in the first section ($\sim\frac{1}{4}$ range) of Al, Ti, and W targets over single-electron calculations and low-intensity beam experiments was observed. The enhancement effect appears to increase with Z. Most of the mechanisms proposed to explain the enhancement effect depend upon dense plasma formation,[11–15] and are probably not applicable at the much lower beam intensity used in these experiments. Indeed, the two-stream plasma instability mechanism yields a Z dependence[3] which is in the opposite direction to our observed results. However, beam stagnation[2,7–10] due to induced magnetic or electric fields in the target could be an explanation of our observed effect at moderate beam intensities. Further theoretical work, extended to this intensity region, would be most helpful.

ACKNOWLEDGMENTS

Discussions with D. W. Rule, A. L. Licht, and M. H. Cha were very helpful. We want to thank E. C. Jones, Jr. and M. Raleigh who participated in portions of this work. We especially want to thank the operating staffs at the NRL linac and the LANL PHERMEX accelerators for their helpful cooperation. This work was supported in part by the U.S. Navy Directed Energy Office.

[1] S. L. Bogolyubskii, B. P. Gerasimov, V. I. Liksonov, Yu. P. Popov, L. I. Rudakov, A. A. Samarskii, V. P. Smirov, and L. I. Urutskoev, Pis'ma Zh. Eksp. Teor. Fiz. **24**, 202 (1976) [JETP Lett. **24**, 178 (1976)].

[2] M. J. Clauser, L. P. Mix, J. W. Poukey, J. P. Quintenz, and A. J. Toepfer, Phys. Rev. Lett. **38**, 398 (1977).

[3] K. Imasaki, S. Miyamoto, S. Higaki, S. Nakai, and C. Yamanaka, Phys. Rev. Lett. **43**, 1937 (1979).

[4] F. C. Young, D. Mosher, S. J. Stephanakis, S. A. Goldstein, and T. A. Mehlhorn, Phys. Rev. Lett. **49**, 549 (1982).

[5] J. W. Tape, W. H. Gibson, J. Remillieux, R. Laubert, and H. E. Wegner, Nucl. Instrum. Methods **132**, 74 (1976).

[6] D. S. Gemmell, J. Remillieux, J. C. Poizat, M. J. Gaillard, R. E. Holland, and Z. Vager, Phys. Rev. Lett. **34**, 1420 (1975).

[7] G. Yonas, J. W. Poukey, K. R. Prestwich, J. R. Freeman, A. J. Toepfer, and M. J. Clauser, Nucl. Fusion **14**, 731 (1974).

[8] D. Mosher, Phys. Rev. Lett. **35**, 851 (1975); D. Mosher and I. B. Bernstein, *ibid.* **38**, 1483 (1977).

[9] M. M. Widner, J. W. Poukey, and J. A. Halbleib, Sr., Phys. Rev. Lett. **38**, 548 (1977).

[10] V. I. Boiko, E. A. Gorbachev, and V. V. Evstigneev, Fiz. Plazmy **9**, 366 (1983) [Sov. J. Plasma Phys. **9**, 213 (1983)].

[11] R. A. McCorkle and G. J. Iafrate, Phys. Rev. Lett. **39**, 1263 (1977).

[12] D. W. Rule, Naval Surface Weapons Center Report No. TR 83-348, (1983); D. W. Rule and M. H. Cha, Phys. Rev. A **24**, 55 (1981).

[13] D. W. Rule and O. H. Crawford, Phys. Rev. Lett. **52**, 934 (1984).

[14] E. Nardi and Z. Zinamon, Phys. Rev. A **18**, 1246 (1978).

[15] S. Nakai, K. Imasaki, and C. Yamanaka, in *Proceedings of the Sixth International Conference on Plasma Physics and Controlled Nuclear Fusion Research, Berchtesgaden, West Germany, 1976* (International Atomic Energy Agency, Vienna, 1977).

[16] J. A. Halbleib, Sr. and T. A. Mehlhorn, Sandia National Laboratory Report No. SAND 84-0573, 1984.

[17] M. J. Berger and S. M. Seltzer, National Bureau of Standards Report No. NBSIR 82-2550-A, 1982.

[18] E. W. Pogue, Los Alamos National Laboratory Report No. LA-UR-84-906B, 1984.

[19] S. M. Seltzer (private communication).

[20] A. Wald and J. Wolfowitz, Ann. Math. Stat. **11**, 147 (1940).

[21] D. C. Moir (private communication).